Accurate model of the stripe domain phase of perpendicularly magnetized multilayers

Ivan Lemesh,* Felix Büttner,† and Geoffrey S. D. Beach
Department of Materials Science and Engineering, Massachusetts Institute of Technology, Cambridge, Massachusetts 02139, USA
(Received 22 December 2016; revised manuscript received 13 April 2017; published 17 May 2017)

We develop an accurate analytical model for the stray field energy of parallel stripe domains in multilayer films with perpendicular magnetic anisotropy, taking into account the effects of finite domain wall width and variable domain wall angle. By minimizing the total energy, we predict the domain width, the domain wall width, and the domain wall angle for given material parameters. We show how the domain wall width depends on the film thickness and the domain size. We explore the domain wall angle as a function of Dzyaloshinskii-Moriya interaction (DMI) and derive a threshold value D_{thr} beyond which the system is in a Néel state. We find that thicker films require larger values of DMI to stabilize the Néel state. Finally, we test the effective medium theory, which allows treating multilayers as effective single layer films, and provide criteria for the applicability of the model in the presence of both surface and volume stray fields. Our results are supported by micromagnetic simulations, which indicate that the predictions are still precise even if the system is in a labyrinthine domain state. Using our model, otherwise inaccessible magnetic parameters, such as the DMI constant or the exchange constant, can now be obtained straightforwardly from static measurements of the stripe domain width in such films.

DOI: 10.1103/PhysRevB.95.174423

I. INTRODUCTION

Magnetic thin films with perpendicular magnetic anisotropy (PMA) play a significant role in modern applications, such as magnetic memory and logic devices. Multidomain patterns in these films form as a competition between various energies, which has been appreciated since the days of Kittel [1]. A number of theoretical approaches based on the so-called wall energy model [2–4] have been presented in the past to describe the energy terms in magnetic thin films and in multilayers. These approaches considered domains separated by sharp domain walls, leading to two competing energy terms: magnetostatic energy and domain wall energy. These terms are crucial for understanding of various magnetic structures formed in the films. The structures themselves, in turn, can play a role in determining the magnetic parameters. For instance, the domain width can be used to measure [5–8] the exchange stiffness A or the Dzyaloshinskii-Moriya interaction (DMI) [9–11] in multilayer films. However, the derivation of magnetic constants from earlier theories, which ignore the internal structure of the domain wall, leads to significant errors. In this paper, we present an analytical model that considers magnetic domains with an accurate domain wall profile, which, unlike earlier theories, also accounts for the magnetostatic interactions between magnetic charges residing within the domain walls. Our model leads to substantial improvements over earlier models at the same level of complexity. In particular, we introduce a thickness dependence of the domain wall width Δ and the domain wall angle ψ, for which we provide simple analytical expressions in Eqs. (20) and (22). In analogy to previous theories, the domain widths of majority and minority stripe domains are obtained from numerical minimization of the total energy function. The revised total energy function of a multilayer film in a multidomain state, as presented in Eq. (31), is the final main result of the paper. Combined, Eqs. (20), (22), and (31) are sufficient for any applications. The interested reader can understand the origin of these equations from the step-by-step derivations presented in the paper and the appendix.

In the wall energy model, the energy density of the wall is assumed to be a constant parameter σ that depends on the magnetic material. The surface stray field energy of the binary stripe state, in which domains are viewed as an alternating sequence of parallel strips, has been calculated for single layer films [3,12] and in multilayers [13,14]. Minimization of the total energy yields the equilibrium domain width W, which depends on domain wall energy σ, saturation magnetization M_s, and film thickness d. The resulting curve $W(d)$ possesses a characteristic minimum and shifts up for larger σ. Additionally, a bubble lattice phase has also been considered [2]. It becomes more stable than the stripe phase above a critical out-of-plane field. A labyrinthine domain pattern, frequently occurring in experiments, has, to the best of our knowledge, not been analyzed so far. The wall energy model is valid only for a bulk material with sharp domain walls, i.e., when $\Delta \ll W$ and $\Delta \ll d$, where Δ is the domain wall width and d is the film thickness. There exist a few corrections to this model, but they only involve the surface stray field energy of a stripe domain state with simplistic linear [15] and sine domain walls [16]. However, studies for stripes with a realistic profile are still absent in the literature. Also, stray field interactions between domain walls have been ignored so far. As we show later in the paper, ignoring these effects for domains of intermediate size ($W < 50\Delta$) leads to wrong values of extracted parameters, such as exchange stiffness or DMI strength.

It is commonly agreed that the profile of straight domain wall (with a domain wall plane orthogonal to the x direction) is analytically described by

$$m_x(x) = \sin(\psi)\cosh^{-1}(x/\Delta), \tag{1}$$

$$m_y(x) = \cos(\psi)\cosh^{-1}(x/\Delta), \tag{2}$$

$$m_z(x) = \tanh(x/\Delta), \tag{3}$$

*ivan.g.lemesh@gmail.com
†felixbuettner@gmail.com

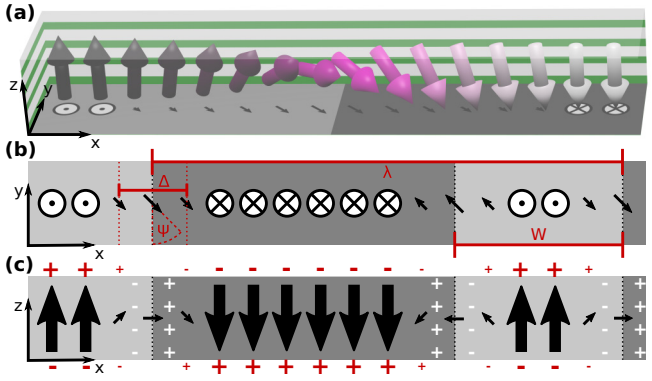

FIG. 1. (a) The profile of a straight domain wall in a multilayer film with arrows denoting the magnetization distribution (adapted from Ref. [17]). (b) Top view and (c) side view of the magnetization in a magnetized multidomain state with domain periodicity λ, domain width W, domain wall width Δ, and domain wall angle ψ. The schematic distribution of surface (volume) charges is depicted with red (white) plus and minus signs.

where $\mathbf{m} = (m_x, m_y, m_z)$ is the normalized magnetization, Δ is the domain wall width, and ψ is the domain wall angle (see Fig. 1). Depending on ψ, the domain walls belong to the Bloch type if $\sin(\psi) = 0$, Néel if $|\sin(\psi)| = 1$, and transient for all other cases. Stripe domains of width W and periodicity λ [see Fig. 1(b)] can be described as a periodic repetition of the single domain wall profile (1)–(3), as long as the distance between the domain walls is at least 8Δ, as shown later in this paper. The magnetostatic energy associated with interactions between volume charges (i.e., the volume stray field energy) formed in a single-wall state with a given profile has been calculated in single layer films and multilayers [17]. The result is a thickness-dependent transverse anisotropy, i.e., a local hard-axis anisotropy that describes the energetic costs to tilt the spins from Bloch to Néel orientation. The surface stray field energy of single walls has been calculated for ultrathin and ultrathick film limits [18,19]. Within those limits, the equilibrium wall parameters can be expressed as

$$\Delta = \sqrt{A/K}, \tag{4}$$

$$\sigma = 4\sqrt{AK}, \tag{5}$$

where K is the local effective anisotropy value, which should not be confused with the total effective magnetic anisotropy energy K_{eff}, as measured from the in-plane and out-of-plane hysteresis loops,[1] [20]. Depending on the film thickness, K can be estimated as

$$K = \begin{cases} K_u - \frac{\mu_0 M_s^2}{2} = K_{\text{eff}} & \text{for ultrathin films,} \\ K_u + \frac{\mu_0 M_s^2}{2}\sin^2(\psi) & \text{for ultrathick films,} \end{cases} \tag{6}$$

where K_u is magnetocrystalline anisotropy. The motivation for these equations comes from the fact that in ultrathin films it is the interaction between surface charges surrounding the domain wall that dominates, while in thicker films volume charge interactions take over.

In this paper, we calculate the equilibrium parameters of an isolated wall with a profile (1)–(3) including the effects of DMI and (surface and volume) stray field energies. We quantitatively predict the Bloch-Néel evolution of the wall as a function of DMI and film thickness. We also consider the multidomain state, calculating its equilibrium domain size and domain wall width. We extend our calculations to multilayers, for which we derive the exact analytical energy expressions and rigorously prove the limits of the previously suggested effective medium approach [5,8,13] with incorporated Zeeman and volume stray field energy effects. We use micromagnetic simulations to confirm our calculations as well as to compare the labyrinthine (mazelike) domains that are more common experimentally, with the binary stripe pattern.

II. CALCULATIONS OF EQUILIBRIUM PARAMETERS

In the following section, we calculate the equilibrium parameters, such as domain wall width Δ, domain wall angle ψ, and domain width W in magnetic films with PMA. We consider a domain wall state described by Eqs. (1)–(3) with demagnetized stripe domains (i.e., the domain periodicity is $\lambda = 2W$). The total energy of the film per unit volume can be summarized as

$$\mathcal{E}_{\text{tot}}^{i,j}(\Delta, W, \psi) = \frac{1}{W}\Big[2\Delta K_u + \frac{2A}{\Delta} + \pi D\sin(\psi) + \sigma_{d,s}^{i,j}(\Delta, W) + \sigma_{d,v}^{i,j}(\Delta, W, \sin(\psi))\Big], \tag{7}$$

where $\sigma_{d,s}^{i,j}$ and $\sigma_{d,v}^{i,j}$ are the surface and the volume stray field energies per domain wall area with i denoting the number of domain walls and j is the number of multilayer repeats. Local energy terms are derived in Appendix A. Here, by D we mean the interfacial DMI constant, although the bulk DMI can be incorporated by adding [21] an extra term $-\pi D_{\text{bulk}}\cos(\psi)$ to Eq. (7). Nonlocal magnetostatic interactions $\sigma_{d,s}^{i,j}$, $\sigma_{d,v}^{i,j}$ can be calculated using the Coulomb integral

$$\mathcal{E}_d^{i,j} = \frac{\mu_0}{8\pi}\iint d^3r\, d^3r'\, \rho_\alpha(\mathbf{r})\rho_\beta(\mathbf{r}')\frac{1}{|\mathbf{r}-\mathbf{r}'|}, \tag{8}$$

with the volume charges $\rho_v = -\nabla\cdot\mathbf{M}$ and the surface charges $\rho_s = (\mathbf{M}\cdot\mathbf{n_k})\delta(z - z_k)$, where $\mathbf{M} = M_s\mathbf{m}$, the index k enumerates the surfaces, and $\mathbf{n_k}$ is the surface normal. The exact solutions for single-wall and multidomain states in single layer and in multilayer systems are provided in Appendixes B and C. The strategy behind all the calculations there is to eliminate the $\mathbf{r} - \mathbf{r}'$ dependency by transforming to Fourier space, in which the integrations become more straightforward. This allows us to eventually reduce a sixfold integral either to an analytical function or to a sum over a single variable. Note that the cross interactions between the surface and the volume

[1] K_{eff}, when defined as the difference in the areas of the in-plane and out-of plane loops, is equal to $K_u - \mu_0 M_s^2/2$ regardless of the film thickness.

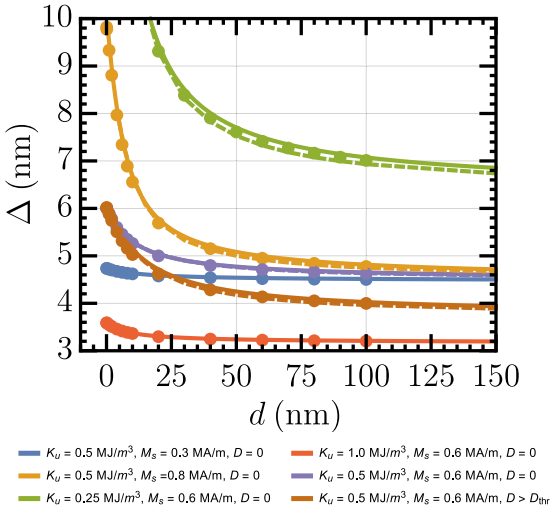

FIG. 2. Domain wall width as a function of film thickness from micromagnetic simulations with 1-nm grid (dots), from numerical solution of the isolated wall theory and from our multidomain theory (dashed).

charges vanish due to the symmetry[2] of our system, i.e.,

$$\mathcal{E}^{i,j}_{d,sv} \equiv 0. \tag{9}$$

The minimization of Eq. (7) with respect to ψ, Δ, W leads to the system of nonlinear equations[3]

$$\begin{aligned} \sin(\psi) &= \tilde{f}\left(-\frac{\pi D}{2\sigma^{i,j}_{d,v}(\psi = 3\pi/2)}\right), \\ \frac{\partial \sigma^{i,j}_{d,s}}{\partial \Delta} + \frac{\partial \sigma^{i,j}_{d,v}}{\partial \Delta} &= \frac{2A}{\Delta^2} - 2K_u, \\ \frac{\partial\left(\sigma^{i,j}_{d,s}/W\right)}{\partial W} + \frac{\partial\left(\sigma^{i,j}_{d,v}/W\right)}{\partial W} &= \frac{2\Delta K_u + \frac{2A}{\Delta} + \pi D \sin(\psi)}{W^2}, \end{aligned} \tag{10}$$

where

$$\tilde{f}(x) = \begin{cases} x, & x \leqslant |1| \\ \mathrm{sgn}(x), & \text{else} \end{cases} \tag{11}$$

with the first equation in (10) stemming from the form of the volume charge interactions $\sigma^{i,j}_{d,v}(\psi, \Delta, W) \equiv \sin^2(\psi)\alpha(\Delta, W)$. Note that the form of the equation allows us to separate the variable ψ from other variables and, hence, reduce the number of independent equations by one. Below, we describe the results of the total energy minimization for single and multilayer films.

[2]For magnetic domains separated by domain walls with the profile from Eqs. (1)–(3), assuming that the chirality and the width of the walls are constant over all layers and domains, the distribution of the surface charges ρ_s is antisymmetric with respect to z, while the distribution of the volume charges ρ_v is a symmetric function with respect to z. Hence, their product is an antisymmetric function and so the mutual interaction between these charges is zero.

[3]In this paper, we choose the domain wall angle and DMI to follow $\sin(\psi) < 0$, $D > 0$ as a convention.

A. Single domain wall

First, consider an isolated domain wall in a single, uniform layer of magnetic material. Figure 2 illustrates the results of the micromagnetic simulations for the equilibrium Δ as a function of film thickness d. We can immediately observe an intrinsic thickness dependence of Δ that is caused by the magnetostatic interactions, which change the local value of anisotropy K in the proximity of the domain wall.

To describe the domain wall profile theoretically, we can use the expression for the stray field energy associated with the volume charges inside of the isolated domain wall obtained by Büttner *et al.* [17]:

$$\sigma^{1,1}_{d,v}(\Delta, \psi) = \frac{\pi \mu_0 M_s^2 \Delta^2 \sin^2(\psi)}{2d} G\left(\frac{d}{2\pi\Delta}\right), \tag{12}$$

with

$$\begin{aligned} G(\alpha) &= \int_0^{+\infty} dq \frac{e^{-q\alpha} + q\alpha - 1}{q \cosh^2(q/4)} \\ &= -8\Big\{\Psi^{-2}(\alpha+1) - \Psi^{-2}\left(\alpha + \frac{1}{2}\right) \\ &\quad - \alpha \ln[\Gamma(\alpha+1)] \\ &\quad + \alpha \ln\left[\Gamma\left(\alpha + \frac{1}{2}\right)\right] - \Psi^{-2}(1) + \Psi^{-2}\left(\frac{1}{2}\right)\Big\}, \end{aligned} \tag{13}$$

where $\Psi^{-2}(z) = \int_0^z dt \, \ln\Gamma(t)$ is the second antiderivative of the digamma function. For the stray field energy of surface charges surrounding the domain wall, we can use the expression that we derive in Appendix B [Eqs. (B11) and (B20)]. Our derivation of the surface stray field energy deals with two domain walls forming a magnetic domain of width W, but we can isolate them by considering the limit $W \to \infty$:

$$\begin{aligned} \sigma^{1,1}_{d,s}(\Delta) &= \lim_{W\to\infty} \sigma^{\Delta}_{d,s} \\ &= \frac{\mu_0 M_s^2}{\pi d}\Big\{\pi d\Delta + \frac{d^2}{2} - d^2 \ln\left(\frac{d}{\pi\Delta}\right) \\ &\quad + 2\pi d\Delta \ln\left[\Gamma\left(\frac{d}{\pi\Delta}\right)\right] - 2\pi^2\Delta^2\Psi^{-2}\left(\frac{d}{\pi\Delta}\right)\Big\}, \end{aligned} \tag{14}$$

where we ignored the term from Eq. (B11), which has no Δ dependence. After the total energy minimization, the first two equations of the system (10) take the form

$$\begin{aligned} \sin(\psi) &= \tilde{f}\left(-\frac{2\pi D}{\Delta\mu_0 M_s^2 G^*\left(\frac{d}{2\pi\Delta}\right)}\right), \\ \frac{\mu_0 M_s^2 \sin^2(\psi)}{8}&\left(1 + \Delta\frac{\partial}{\partial\Delta}\right)G^*\left(\frac{d}{2\pi\Delta}\right) + \frac{1}{2}\frac{\partial\sigma^{1,1}_{d,s}}{\partial\Delta} \\ &= \frac{A}{\Delta^2} - K_u, \end{aligned} \tag{15}$$

where $G^*(x) = G(x)/x$. By inserting $\sin(\psi)$ from the first equation in system (15) into the second one, we obtain an

expression that depends only on Δ.[4] In the limit of small and large d, the resulting system can be expanded in series, which leads to the following explicit form for the equilibrium domain wall width:

$$\lim_{d\to 0}\Delta = \Delta_0 - \frac{\mu_0 M_s^2}{4\pi K_{\text{eff}}}d, \tag{16}$$

$$\lim_{d\to\infty}\Delta = \Delta_\infty = \sqrt{\frac{A}{K_u + \frac{\mu_0 M_s^2}{2}\sin^2(\psi)}}, \tag{17}$$

where

$$\Delta_0 = \sqrt{\frac{A}{K_{\text{eff}}}}, \tag{18}$$

$$K_{\text{eff}} = K_u - \frac{\mu_0 M_s^2}{2}. \tag{19}$$

Although the exact solutions for films of an intermediate thickness can be found only numerically, we can use the fact that the resulting Δ is a linear function of d for ultrathin films and a constant function for ultrathick films and approximately extrapolate Δ to the intermediate thickness regime as follows:

$$\Delta(d,\psi) = \Delta_0 - \frac{1}{\frac{2\pi(Q-1)}{d} + \frac{1}{\Delta_0 - \Delta_\infty(\psi)}}, \tag{20}$$

with the quality factor Q being defined as

$$Q = \frac{2K_u}{\mu_0 M_s^2}. \tag{21}$$

The domain wall width as described by the simplified explicit Eq. (20) accurately represents the exact implicit result of Eq. (15), unless Q is very close to one. Specifically, we find that in the intermediate thickness regime the relative error of Eq. (20) is below 10% for $Q \geqslant 1.2$, with the error decreasing rapidly for larger Q. For thin and thick films, Eq. (20) becomes precise for any $Q > 1$.

The domain wall width implicitly depends on DMI [Fig. 3(a)] via the $\psi = \psi(D)$ dependence of Δ. Such a dependence exists only for transient walls, in which the contribution of the volume stray field energy depends on the domain wall angle ψ. After plotting the numerical solution for $\sin(\psi)$ [Fig. 3(b)], we can see that thicker films require larger values of DMI in order to stabilize Néel walls. The transient regime spreads from DMI values of zero, at which the domain wall has a Bloch profile, up to some threshold value D_{thr} of DMI. Once $D = D_{\text{thr}}$, a transient wall becomes purely Néel. A further increase of DMI leads to no change of domain wall width Δ as a function of DMI.

D_{thr} can be found by imposing the Néel character of the walls, i.e., by plugging $|\sin(\psi)| = 1$ into Eq. (15). The resulting numerical solution is plotted in Fig. 4(a). We can derive the ultrathick and ultrathin film limits of D_{thr} and the equilibrium ψ by inserting the analytical limits of the equilibrium Δ from Eqs. (16) and (17) into the first equation in the system (15). Just like in the case of Δ, we can use these

[4]This is an implicit equation for Δ.

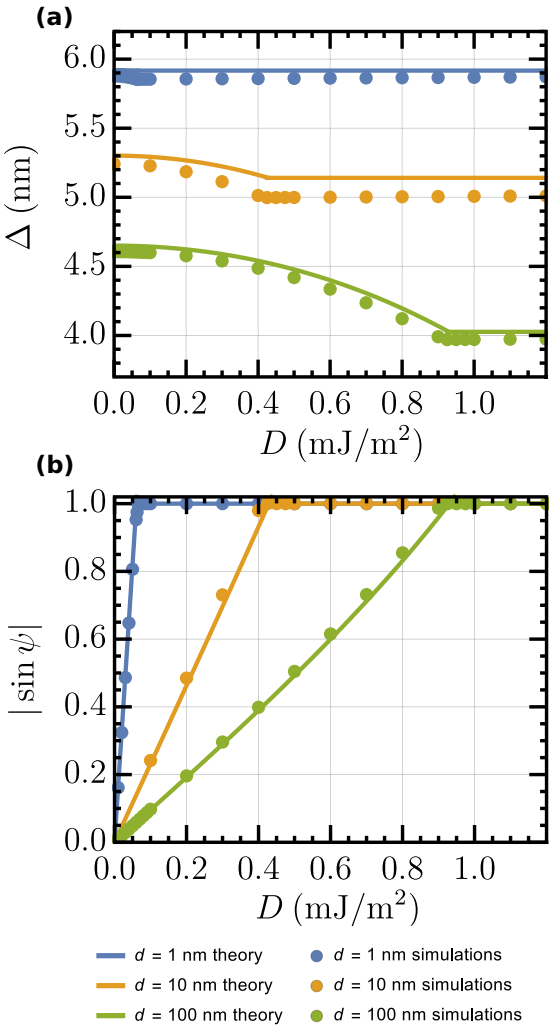

FIG. 3. The values of equilibrium domain wall width Δ and domain wall angle $\sin(\psi)$ as a function of DMI for an isolated wall in an infinite single layer film with material parameters: $A = 1.0 \times 10^{-11}$ J/m, $M_s = 6.0 \times 10^5$ A/m, $K_u = 5.0 \times 10^5$ J/m^3. Continuous curves represent theoretical values, corresponding to the exact numerical solutions of (15), while dots represent single layer micromagnetic simulations, with a slight mismatch caused by a finite-cell size.

solutions to approximate the equilibrium ψ and D_{thr} in the entire film thickness range as follows:

$$\sin(\psi) = \begin{cases} -D/D_{\text{thr}}, & |D| < D_{\text{thr}} \\ -\text{sgn}(D), & |D| \geqslant D_{\text{thr}} \end{cases} \tag{22}$$

$$D_{\text{thr}}(d) = \frac{2\mu_0 M_s^2}{\frac{\pi^2}{d\ln(2)} + \pi\sqrt{\frac{K_u + \frac{\mu_0 M_s^2}{2}}{A}}}. \tag{23}$$

To further confirm our predictions, we performed a series of micromagnetic simulations with MUMAX3 micromagnetic software [22]. We used a fine monolayer grid of 1 nm in lateral directions and the number of cells $(N_x, N_y, N_z) = (32\,768 \times 512 \times 1)$, in which we applied the periodic boundary conditions to remove the influence of boundary effects [23] caused by DMI. By starting from an isolated

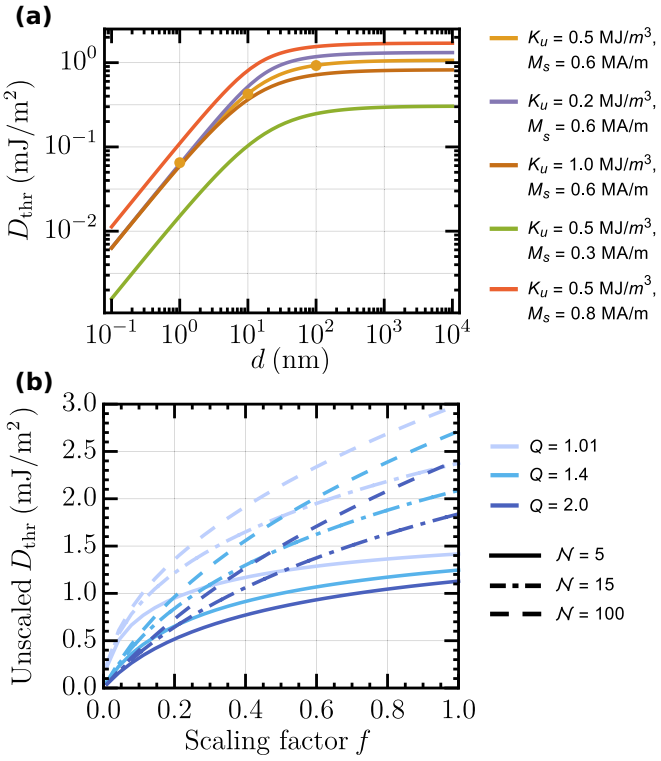

FIG. 4. Theoretical values of the threshold DMI. (a) D_{thr} as a function of film thickness for single layer films. The dots indicate the results from 1-nm-grid micromagnetic simulations with varying the DMI, where D_{thr} was found from the minimum D, yielding a Néel state. (b) D_{thr} as a function of scaling factor $f = \mathcal{T}/\mathcal{P}$ for multilayer films (via the effective medium model) with single magnetic layer thickness $\mathcal{T} = 1$ nm, and unscaled magnetic parameters $M_s = 1.4 \times 10^6$ A/m, $A = 1.0 \times 10^{-11}$ J/m, for different values of magnetic layer quality factor $Q = 2K_u/\mu_0 M_s^2$ and multilayer repeats $\mathcal{N}$.

transient wall state, we further relaxed it until the minimum energy state was reached. Such simulations precisely confirm the equilibrium Δ and ψ obtained numerically from Eq. (15).

B. Extension to stripes

Consider a single, uniform layer of a magnetized film with a periodic domain pattern with a periodicity λ, minority domain width of W, and domain wall width Δ (see Fig. 2). In Appendixes B 2 and C 1, we calculate for the surface and volume stray field of such a state, resulting in the following expressions normalized per unit volume of the film:

$$\mathcal{E}_{d,s}^{\infty,1} = \frac{\mu_0 M_s^2}{2}\left(1-\frac{2W}{\lambda}\right)^2 + \frac{2\pi\mu_0 M_s^2\Delta^2}{\lambda d} \times \sum_{n=1}^{\infty} \frac{\sin^2\left(\frac{\pi n W}{\lambda}\right)}{\sinh^2\left(\frac{\pi^2 n\Delta}{\lambda}\right)} \frac{1-\exp\left(-\frac{2\pi n d}{\lambda}\right)}{n}, \quad (24)$$

$$\mathcal{E}_{d,v}^{\infty,1} = \frac{2\pi\mu_0 M_s^2\Delta^2\sin^2(\psi)}{\lambda d} \times \sum_{n=1}^{\infty} \frac{\sin^2\left(\frac{\pi n W}{\lambda}\right)}{\cosh^2\left(\frac{\pi^2 n\Delta}{\lambda}\right)} \frac{\exp\left(-\frac{2\pi n d}{\lambda}\right)+\frac{2\pi n d}{\lambda}-1}{n}. \quad (25)$$

We can find the equilibrium values of W and Δ after incorporating the magnetostatic energies $\mathcal{E}_{d,s}^{\infty,1}$ and $\mathcal{E}_{d,v}^{\infty,1}$ into the total energy expression

$$\mathcal{E}_{\text{tot}}^{\infty,1} = \frac{2}{\lambda}\left[\frac{2A}{\Delta} + 2K_u\Delta + \pi D\sin(\psi)\right] + \mathcal{E}_{d,s}^{\infty,1}(M_s,d,\lambda,W,\Delta) + \mathcal{E}_{d,v}^{\infty,1}(M_s,d,\lambda,W,\Delta,\psi) - M_s\left(1-\frac{2W}{\lambda}\right)B_z, \quad (26)$$

where B_z is the component of the external field along the magnetization direction. Considering a demagnetized state $W = \lambda/2$, the minimization of Eq. (26) with respect to W, Δ, ψ leads to Eq. (10). Figure 5 shows the results of the numerical minimization procedure, i.e., the equilibrium domain width is plotted as a function of film thickness for a material with $Q > 1$.

The equilibrium domain width $W = W(d)$ possesses a minimum as a function of film thickness, enclosed by a slow increase of W towards larger d and a sharp increase (divergence) for thinner films. Qualitatively, such a trend is in agreement with theories developed earlier [3], which used a constant wall energy model. Quantitatively, however, earlier theories possess an inherent error as they completely ignore the thickness dependence of the domain wall energy and neglect the interwall interactions. These errors are addressed in the multidomain model that we developed.

Our explicit model can be simplified using the following approximation: (i) use Δ, ψ found from the derived single-wall model [Eqs. (20) and (22)], (ii) plug them into the total energy [Eq. (26)], and (iii) minimize it with respect to a single variable W. This approach is valid (see Fig. 5, dotted-dashed curve) because the equilibrium Δ depends on the domain size W only weakly (dashed lines on Fig. 2).

Note that the DMI interaction leads to the shrinking of the domain size by lowering the energetic cost of the formation of domain walls. Above some critical DMI, $D_{\text{cr}} \neq D_{\text{thr}}$, the multidomain state evolves into a cycloid state [23]. It is hence useful to compare our theoretical results with micromagnetic stripe simulations at extremes. The limits of our theory can be tested by tuning DMI to the point at which the size of the domain becomes equal to the domain wall width. From Fig. 6 we can see that our theory works well as long as $W \gtrsim 8\Delta$. Real domains rarely exceed this limit, so our theory holds true for the majority of experimentally relevant cases.

Our calculations are verified by micromagnetic simulations that reproduce the desired values for W, Δ, and ψ (Fig. 7, dots and stars in Fig. 5). In addition, simulations show that those parameters are also the same if the system is in a state of randomly oriented labyrinthine domains. We attribute contradicting experimental observations [24,25] to the effect of pinning.

C. Extension to multilayers and revised effective medium approach

Now, consider multidomain patterns in a multilayer structure, which has $\mathcal{N}$ multilayer repeats with a stack periodicity $\mathcal{P}$ and a single magnetic layer thickness $\mathcal{T}$. In Appendixes B 3 and C 2, we provide the exact solution of Eq. (8) for the surface $\sigma_{d,s}^{\infty,\mathcal{N}}$ and volume $\sigma_{d,v}^{\infty,\mathcal{N}}$ stray field energies [see Eqs. (B34)

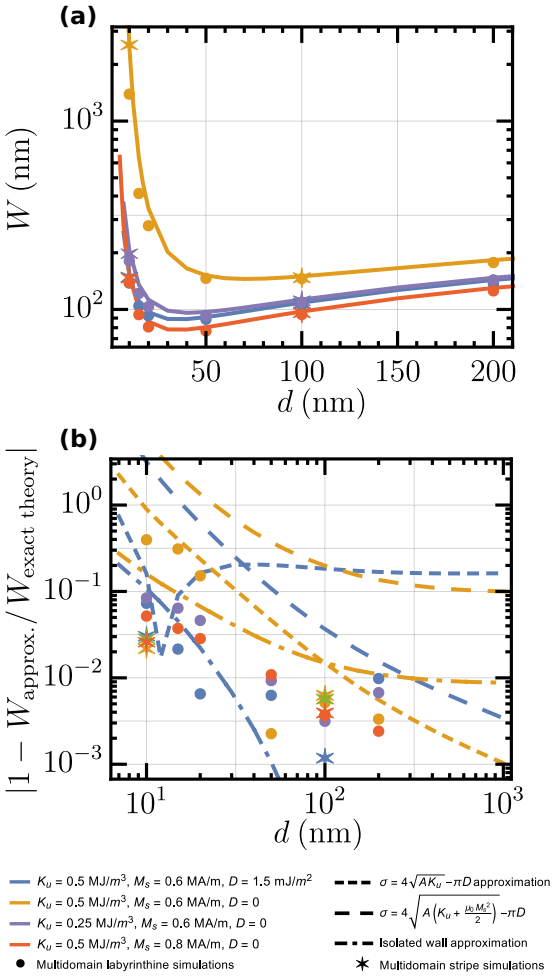

FIG. 5. (a) Equilibrium domain width at remanence as a function of film thickness for films with a single magnetic layer: from the exact theory and from the micromagnetic simulations of the labyrinthine and stripe state (see also Fig. 7). (b) Mismatch between various multidomain approximations, micromagnetic simulations, and our multidomain theory. Our theory uses the numerical minimization of Eq. (10). The models that we compare it against are constant wall energy models (depicted with dashed lines), and the isolated wall approximation to our multidomain theory (shown with a dotted-dashed line), which uses Δ and ψ found from the single-wall model [Eq. (15)], followed by the minimization of Eq. (26) with respect to a single variable W. Note that the thin film deviation of simulation results from our predictions originates in the quantization due to a finite simulation area, which is more restricting for larger domain sizes, i.e., smaller film thicknesses.

and (C24)]. We thus provide the reader with all the tools to find the equilibrium multilayer parameters λ, W, Δ, ψ, which can be accomplished by minimizing the total energy

$$\begin{aligned}\mathcal{E}_{\text{tot}}^{\infty,\mathcal{N}} = {} & \frac{2}{\lambda}\left[\frac{2A}{\Delta}f + 2K_u\Delta f + \pi D\sin(\psi)f\right] \\ & + \mathcal{E}_{d,s}^{\infty,\mathcal{N}}(M_s,\mathcal{T},\mathcal{P},\lambda,W,\Delta) \\ & + \mathcal{E}_{d,v}^{\infty,\mathcal{N}}(M_s,\mathcal{T},\mathcal{P},\lambda,W,\Delta,\psi) \\ & - M_s\left(1-\frac{2W}{\lambda}\right)B_z f, \end{aligned} \tag{27}$$

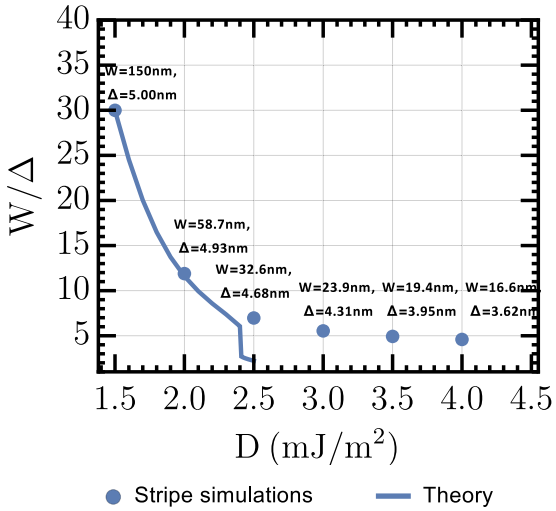

FIG. 6. The ratio of the equilibrium domain size W and domain wall width Δ as a function of DMI for states with Néel walls ($D > D_{\text{thr}} \approx 1.0\times10^{-3}$ J/m^2) following the developed theory and multidomain stripe simulations with $d = 10$ nm, $A = 1.0\times10^{-11}$ J/m, $M_s = 6.0\times10^5$ A/m, $K_u = 5.0\times10^5$ J/m^3.

where $\mathcal{E}_{d,s}^{\infty,\mathcal{N}}$, $\mathcal{E}_{d,v}^{\infty,\mathcal{N}}$ are defined as follows:

$$\begin{aligned}\mathcal{E}_{d,s}^{\infty,\mathcal{N}} = {} & \frac{\mu_0 M_s^2}{2}\left(\frac{2W}{\lambda}-1\right)^2\frac{\mathcal{T}}{\mathcal{P}} \\ & + \frac{2\pi\mu_0 M_s^2\Delta^2}{\lambda\mathcal{P}}\sum_{n=1}^{\infty}\frac{\sin^2\left(\frac{\pi n W}{\lambda}\right)}{n\sinh^2\left(\frac{\pi^2 n\Delta}{\lambda}\right)}\end{aligned}$$

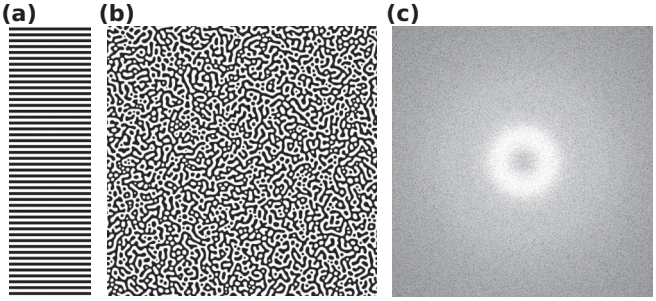

FIG. 7. Simulated demagnetized multidomain patterns of a material with $A = 1.0\times10^{-11}$ J/m, $M_s = 6.0\times10^5$ A/m, $K_u = 5.0\times10^5$ J/m^3, $D = 1.5\times10^{-3}$ J/m^2 with applied periodic boundary conditions. (a) Binary stripe pattern (10 μm $\times$ 3 μm) which was selected after comparing the total energies of the simulated states with various number of stripes and finding the one that results in the smallest total energy (after the relaxation procedure), with the cell size of 1 nm $\times$ 1 nm $\times$ 100 nm. The true domain width at the absolute energy minimum can be found after fitting the parabolic discrete curve $E_{\text{tot}} = E_{\text{tot}}(N_{\text{stripes}})$ and locating the minimum of the resulting curve. (b) Labyrinthine (maze) pattern (10 μm $\times$ 10 μm) that was found after the relaxation procedure of a randomly magnetized state; the cell size is 2 nm $\times$ 2 nm $\times$ 100 nm. (c) FFT of the respective state (magnified 10$\times$) used for measuring domain width W at equilibrium.

$$\times \left\{ \frac{2\sinh\left(\frac{\pi n\mathcal{T}}{\lambda}\right)\sinh\left(\frac{\pi n(\mathcal{P}-\mathcal{T})}{\lambda}\right)}{\sinh\left(\frac{\pi n\mathcal{P}}{\lambda}\right)} + \frac{\sinh^2\left(\frac{\pi n\mathcal{T}}{\lambda}\right)}{\mathcal{N}\sinh^2\left(\frac{\pi n\mathcal{P}}{\lambda}\right)}\left(1-e^{-\frac{2\pi\mathcal{P}\mathcal{N}n}{\lambda}}\right)\right\}, \quad (28)$$

$$\mathcal{E}_{d,v}^{\infty,\mathcal{N}} = \frac{2\pi\mu_0 M_s^2\Delta^2\,\sin^2(\psi)}{\lambda\mathcal{P}\mathcal{N}}\sum_{n=1}^{\infty}\frac{\sin^2\left(\frac{\pi nW}{\lambda}\right)}{n\cosh^2\left(\frac{\pi^2 n\Delta}{\lambda}\right)} \times \left\{\mathcal{N}\left(e^{-\frac{2\pi n\mathcal{T}}{\lambda}}+\frac{2\pi n\mathcal{T}}{\lambda}-1\right) + \frac{e^{-\frac{2\pi n(\mathcal{P}\mathcal{N}+\mathcal{T})}{\lambda}}\left(e^{\frac{2\pi n\mathcal{T}}{\lambda}}-1\right)^2}{\left(e^{\frac{2\pi n\mathcal{P}}{\lambda}}-1\right)^2} \times \left(e^{\frac{2\pi n\mathcal{P}}{\lambda}}+e^{\frac{2\pi n\mathcal{P}(\mathcal{N}+1)}{\lambda}}(\mathcal{N}-1)-\mathcal{N}e^{\frac{2\pi n\mathcal{N}\mathcal{P}}{\lambda}}\right)\right\}. \quad (29)$$

However, at this point the explicit energy expressions become too involved. Instead, we prove and test a single layer *effective medium model* [5,8,13]. In accordance with this model, the multilayers can be effectively treated as a single layer film with thickness $d = \mathcal{N}\mathcal{P}$ with magnetic constants scaled by a factor $f = \frac{\mathcal{T}}{\mathcal{P}}$ [8,13]. Such a model has been introduced previously, but neither a rigorous proof nor the limits of validity have been discussed. The error of the equilibrium domain width, extracted from the effective medium model, is plotted in Fig. 8. As we find in Appendixes B 3 and C 2, the effective medium model is accurate if $W \gg \mathcal{P}$, $W \gg \Delta$ (imposed by the surface stray field energy) and $\mathcal{P} \ll 2\pi\Delta$ (imposed by the volume stray field energy). The conditions are met in most experimentally relevant cases. At these limits, the surface stray field energy not only scales M_s by a factor f, but also generates an additional anisotropylike offset term K_a [see Eq. (B38)] defined as

$$K_a = \frac{\mu_0 M_s^2}{2}(f-f^2)\left(1-\frac{4\Delta}{\lambda}\right) \quad \text{at } 2\Delta/\lambda \to 0, \quad (30)$$

which results in modifying the magnetocrystalline energy term as well as in making a constant energy offset. The volume stray field energy density, as we demonstrate in Appendix C 2, should be scaled by a factor f^2, which is equivalent to the scaling of M_s by the factor f. Overall, we can express the energy of the mutidomain multilayers in the effective medium model as follows:

$$\mathcal{E}_{\text{tot, eff}}^{\infty,\mathcal{N}} = \frac{2}{\lambda}\left[\frac{2A'}{\Delta}+2K_u'\Delta+\pi D'\sin(\psi)\right] + \mathcal{E}_{d,s}^{\infty,1}(M_s=M_s',d=\mathcal{P}\mathcal{N}) + \mathcal{E}_{d,v}^{\infty,1}(M_s=M_s',d=\mathcal{P}\mathcal{N}) + C - M_s'\left(1-\frac{2W}{\lambda}\right)B_z, \quad (31)$$

where the effective constants are defined as

$$A' = fA, \quad D' = fD, \quad M_s' = fM_s, \quad (32)$$

$$K_u' = K_u f - \frac{\mu_0 M_s^2}{2}(f-f^2), \quad C = \frac{\mu_0 M_s^2}{2}(f-f^2). \quad (33)$$

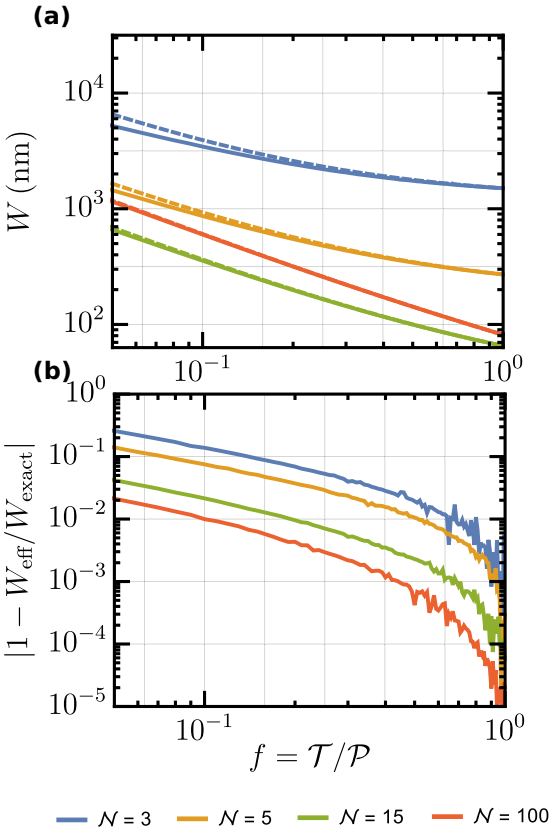

FIG. 8. Equilibrium domain width as a function of scaling factor f and the number of multilayer repeats $\mathcal{N}$ for a multilayer film with magnetic layer of thickness $\mathcal{T} = 1$ nm, and magnetic parameters $M_s = 1.4 \times 10^6$ A/m, $K_u = 2.7 \times 10^6$ J/m^3, $A = 1.0 \times 10^{-11}$ J/m, $D = 1.5 \times 10^{-3}$ J/m^2. Solid lines represent the explicit multilayer theory solution, dashed lines are the effective medium approximation. The minimum domain width is reached at the number of multilayer repeats $\mathcal{N} \approx 15$. The equilibrium domain wall width (not shown) ranges from $\Delta \sim 2.5$ nm for small f to $\Delta \sim 1.7$ nm for films with large f.

The form of the scaling of magnetocrystalline anisotropy term K_u obtained in the Eq. (33) is equivalent to the claim by Woo *et al.* [8] that the effective anisotropy $K_{\text{eff}} = K_u - \frac{\mu_0 M_s^2}{2}$ should be scaled by a factor f. Also, the derived constant term C is equivalent to an extra surface stray field energy term found by Suna [13] in a multilayer binary domain pattern.

III. CONCLUSIONS

We have developed a theory to calculate the equilibrium domain size W, domain wall width Δ, and domain wall angle ψ in multilayers possessing a multidomain state with an accurate profile of domain walls. This theory can be used inversely to find material parameters such as DMI or exchange stiffness from the known domain width. We have also verified the validity of the effective medium model, which allows treating multilayers effectively as a single layer film, and have found the limitations of the model for multidomain multilayers. Using micromagnetic simulations, we have found that the labyrinthine and stripe phases result in very close values of the equilibrium domain width.

ACKNOWLEDGMENTS

This work was supported by the U. S. Department of Energy (DOE), Office of Science, Basic Energy Sciences (BES) under Award No. DE-SC0012371. F.B. acknowledges support by the German Research Foundation through Award No. BU 3297/1-1.

I.L. and F.B. contributed equally to this work.

APPENDIX A: LOCAL ENERGY TERMS

To express the local energy terms of the isolated wall state per domain wall area, we need to integrate the well-known expressions of micromagnetic energy densities using the one-dimensional magnetization profiles (1)–(3). Thus, the energy of magnetocrystalline anisotropy, exchange interaction, and DMI [11,21] per domain wall area can be found as follows:

$$\sigma_k = K_u \int_{-\infty}^{+\infty} dx[(m_x)^2 + (m_y)^2] = 2\Delta K_u, \tag{A1}$$

$$\sigma_{\text{exch}} = A \int_{-\infty}^{+\infty} dx \left[\left(\frac{m_x}{\partial x}\right)^2 + \left(\frac{m_y}{\partial x}\right)^2 + \left(\frac{m_z}{\partial x}\right)^2 \right] = \frac{2A}{\Delta}, \tag{A2}$$

$$\sigma_{\text{DMI}} = D \int_{-\infty}^{+\infty} dx \left[m_x \frac{\partial m_z}{\partial x} - m_z \frac{\partial m_x}{\partial x} \right] = \pi D \sin(\psi). \tag{A3}$$

APPENDIX B: SURFACE STRAY FIELD ENERGY CALCULATIONS

1. Single-domain case

A single stripe domain is an area of width W separated by domain walls. The profile of the normalized out-of-plane component of the local magnetization $m_z(\mathbf{r}) = m_z(x)$ can be written as

$$m_z(x) = 1 - \tanh\left(\frac{W+2x}{2\Delta}\right) - \tanh\left(\frac{W-2x}{2\Delta}\right) \tag{B1}$$

$$= (f_1 * g)(x) \tag{B2}$$

with

$$g(x,W) = \begin{cases} -1 & |x| < W/2, \\ 1 & \text{else}, \end{cases} \tag{B3}$$

$$f_1(x,\Delta) = \frac{1}{2\Delta} \frac{1}{\cosh^2(x/\Delta)}. \tag{B4}$$

The unit box function $g(x,W)$ is a model for a domain of width W with zero domain wall width and the convolution with the $f_1(x,\Delta)$ yields a finite domain wall width Δ. The function for $m_z(x)$ is not an exact model for a 360° domain wall [26], but it is a very accurate approximation for $W > 8\Delta$. The out-of-plane component of the magnetization determines the surface charge density via

$$\rho_s(\mathbf{r}) = [\delta(z-d) - \delta(z)] M_s m_z(\mathbf{r}), \tag{B5}$$

where d is the film thickness, M_s is the saturation magnetization. The in-plane components m_x and m_y do not generate surface charges and the interaction of surface charges and volume charges is zero in the average over z.[5] In general, the stray field energy $E_{d,s}$ related to surface charges of density $\rho_s(\mathbf{r})$ can be calculated via the integral

$$E_{d,s} = \frac{\mu_0}{8\pi} \iint d^3r\, d^3r' \rho_s(\mathbf{r}) \rho_s(\mathbf{r}') \frac{1}{|\mathbf{r} - \mathbf{r}'|}. \tag{B6}$$

In the following, we express our results in terms of the energy per unit area of the domain wall

$$\sigma_{d,s} = \frac{E_{d,s} - E_0}{2Ld}, \tag{B7}$$

where L is the length of the domain, measured in the y direction, and E_0 is the energy of a homogeneously magnetized film. The factor 2 in the denominator comes from the fact that the domain has two domain walls. With the tools provided in Ref. [17], the integration along y and z can be performed analytically. In the limit $L \to \infty$, the integration kernel reads as

$$h(x,d) = \lim_{L\to\infty} \frac{1}{2L} \iint_{-L/2}^{L/2} dy\, dy' \iint_0^d dz\, dz' \times \frac{[\delta(z-d) - \delta(z)][\delta(z'-d) - \delta(z')]}{\sqrt{x^2 + (y-y')^2 + (z-z')^2}} \tag{B8}$$

$$= \ln(x^2 + d^2) - \ln(x^2). \tag{B9}$$

With the help of $h(x)$, we can write $\sigma_{d,s}$ as

$$\sigma_{d,s} = \frac{\mu_0 M_s^2}{8\pi d} \iint dx\, dx' \times [(f_1 * g)(x)(f_1 * g)(x') - 1] h(x - x', d). \tag{B10}$$

The -1 represents the subtraction of the stray field energy of a homogeneously magnetized film. Because of the -1 term, it is difficult to write the integral in Fourier space. However, by further subtracting the known stray field energy [2] of a stripe domain with zero domain wall width

$$\sigma_{d,s}^0 = \frac{\mu_0 M_s^2}{8\pi d} \iint dx\, dx' [g(x)g(x') - 1] h(x - x', d)$$

$$= -\mu_0 M_s^2 d v \left\{ 1 - (2\pi)^{-1} \left[4 \arctan(v) - 2v \ln(v) + \left(v - \frac{1}{v}\right) \ln(v^2 + 1) \right] \right\}, \tag{B11}$$

where $v = W/d$, we can write the difference

$$\sigma_{d,s}^{\Delta} = \sigma_{d,s} - \sigma_{d,s}^0 = \frac{\mu_0 M_s^2}{8\pi d} \sqrt{2\pi} \int dk \left[2\pi \hat{f}_1^{\,2}(k) - 1 \right] \hat{g}^2(k) \hat{h}(k,d) \tag{B12}$$

as a single integral in Fourier space [17]. Here, the hat above the functions denotes a Fourier transform

$$\hat{f}_1(k) = \frac{1}{\sqrt{2\pi}} \int dx\, f_1(x) e^{ikx}. \tag{B13}$$

[5] If we assume the spin structure to be uniform along the z direction.

To derive Eq. (B12), we made use of the fact that

$$\mathcal{F}(f_1 * g)(k) = \sqrt{2\pi}\,\hat{f}_1(k)\hat{g}(k) \tag{B14}$$

and that both $\hat{f}_1$ and $\hat{g}$ are real valued. The Fourier space functions are

$$2\pi\,\hat{f}_1^{\,2}(k) = \frac{\pi^2}{4}\Delta^2 k^2 \frac{1}{\sinh^2\left(\frac{\pi\Delta k}{2}\right)}, \tag{B15}$$

$$\hat{g}^2(k) = \frac{8}{\pi}\frac{1}{k^2}\sin^2\left(\frac{kW}{2}\right), \tag{B16}$$

$$\hat{h}(k,d) = \sqrt{2\pi}\,\frac{1-\exp(-|k|d)}{|k|}. \tag{B17}$$

Actually, the Fourier transform of g contains more terms proportional to $\delta(k)$, but those terms integrate to zero because the remaining integrand is zero at $k = 0$. All together, the equation for $\sigma^{\Delta}_{d,s}$ reads as

$$\sigma^{\Delta}_{d,s} = 4\frac{\mu_0 M_s^2}{\pi d}\Delta^2 \int_0^\infty dq \left(\frac{\pi^2}{4}q^2\frac{1}{\sinh^2\left(\frac{\pi q}{2}\right)} - 1\right) \times \sin^2\left(\frac{qw}{2}\right)\frac{1-\exp(-qt)}{q^3}, \tag{B18}$$

where we substituted $q = k\Delta$, reduced the symmetric integral to positive values of q, and introduced the new variables $t = d/\Delta$ and $w = W/\Delta$. The integral can be solved analytically by noting that $1 - e^{-qt} = \int_0^t q e^{-qx}\,dx$, changing the order of the q and x integration, and using the fact that

$$\int_0^\infty dq\,\pi^2\frac{\sin^2\left(\frac{qw}{2}\right)}{\sinh^2\left(\frac{\pi q}{2}\right)}\exp(-qx) = i(w+ix)\Psi\left(\frac{x-iw}{\pi}\right) + (-x-iw)\Psi\left(\frac{iw+x}{\pi}\right) + 2x\Psi\left(\frac{x}{\pi}\right). \tag{B19}$$

The result is

$$\sigma^{\Delta}_{d,s} = \frac{\mu_0 M_s^2\Delta}{2\pi}(a - 2\pi b - 2\pi^2 t^{-1}c), \tag{B20}$$

$$a = 4\pi\,\log\Gamma\left(\frac{t}{\pi}\right) + t[2v^2\log(v) - (v^2-1)\log(v^2+1) - 4v\arctan(v)], \tag{B21}$$

$$b = -iv\log\Gamma\left(\frac{itv}{\pi}\right) + (1+iv)\log\Gamma\left(\frac{ivt+t}{\pi}\right) + (1-iv)\log\Gamma\left(\frac{t-itv}{\pi}\right) + iv\log\Gamma\left(-\frac{itv}{\pi}\right), \tag{B22}$$

$$c = \Psi^{(-2)}\left(\frac{itv}{\pi}\right) - \Psi^{(-2)}\left(\frac{ivt+t}{\pi}\right) - \Psi^{(-2)}\left(\frac{t-itv}{\pi}\right) + \Psi^{(-2)}\left(-\frac{itv}{\pi}\right) + 2\Psi^{(-2)}\left(\frac{t}{\pi}\right), \tag{B23}$$

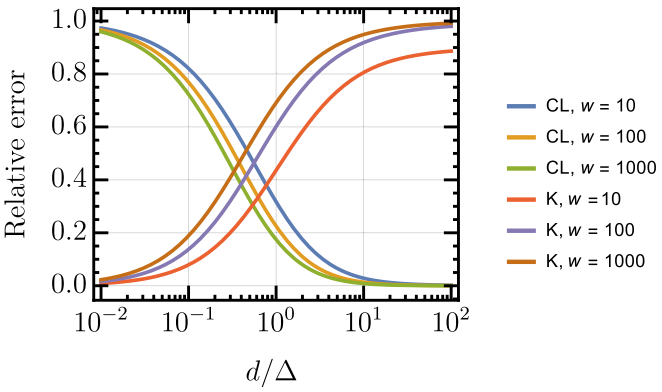

FIG. 9. Relative error for using the zero wall width model of Cape and Lehman (CL) and for using the thin film limit effective anisotropy model (K).

where i is the imaginary unit, Γ is the gamma function, and $\Psi^{-2}(z) = \int_0^z dt\,\ln\Gamma(t)$ is the second antiderivative of the digamma function.

The error made by using the binary approximation $\sigma^0_{d,s}$ instead of the correct $\sigma^0_{d,s} + \sigma^{\Delta}_{d,s}$ is

$$\Delta\sigma^0_{d,s} = \frac{\sigma^{\Delta}_{d,s}}{\sigma^{\Delta}_{d,s} + \sigma^0_{d,s}}. \tag{B24}$$

The error made by using the thin film effective anisotropy model

$$\sigma^K_{d,s} = -\mu_0 M_s^2\Delta \tag{B25}$$

is

$$\Delta\sigma^K_{d,s} = 1 - \frac{\sigma^K_{d,s}}{\sigma^{\Delta}_{d,s} + \sigma^0_{d,s}}. \tag{B26}$$

Both errors are plotted in Fig. 9 as a function of reduced thickness t for various values of w. For a given thickness, $\Delta\sigma^0_{d,s}$ vanishes when W becomes large, but logarithmically slow. For typical domain widths, i.e., for $10 < w < 1000$, we show that there is a significant error $\Delta\sigma^0_{d,s}$ of 10% and more for $t < 3$. The thin film approximation, on the contrary, is reasonably accurate only for small $t < 0.1$. For the important intermediate

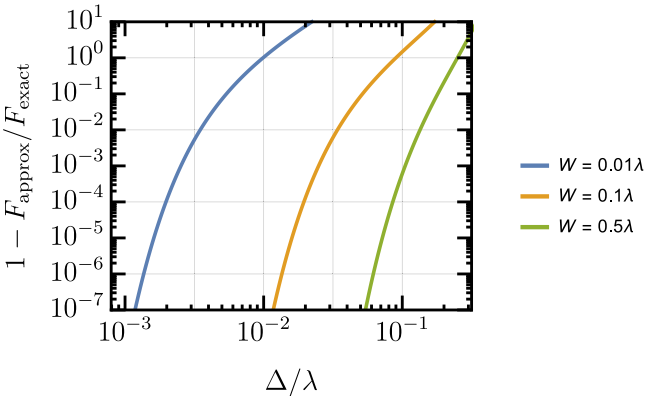

FIG. 10. The error of the asymptotic approximation of $F(\frac{\Delta}{W})$ for various values of minority domain size.

regime $0.1 < t < 3$, the full term $\sigma_{d,s} = \sigma_{d,s}^{\Delta} + \sigma_{d,s}^{0}$ needs to be considered. Note that both approximations underestimate the correct result.

2. Extension to stripe arrays

Consider a periodic stripe domain pattern with periodicity λ and a width W of one of the domains. To start with, consider a finite number of domains N and a finite total width of the sample of $N\lambda$. The effective domain wall energy associated with the surface stray fields is then given by

$$\sigma_{d,s} = \frac{E_{d,s}}{2NLd}. \tag{B27}$$

With the help of the identities derived in Appendix D, $\sigma_{d,s}$ can be written as

$$\sigma_{d,s} = \sqrt{2\pi}\frac{\mu_0 M_s^2 \lambda}{8\pi d}\sum_k |\hat{g}_k|^2 \hat{h}(k). \tag{B28}$$

For a square wave domain pattern with zero domain wall width, the Fourier coefficients of g are [3]

$$|\hat{g}_k|^2 = \frac{32}{\lambda^2 k^2}\sin^2\left(\frac{kW}{2}\right) = 4\pi|\hat{g}(k)|^2 \tag{B29}$$

with $k = 2\pi n/\lambda$ and $n \in \mathbb{N}\backslash 0$ and

$$|\hat{g}_0|^2 = \left(\frac{2W}{\lambda} - 1\right)^2. \tag{B30}$$

All together,

$$\sigma_{d,s} = \frac{\lambda}{4}\mu_0 M_s^2\left(\frac{2W}{\lambda} - 1\right)^2 + \frac{\mu_0 M_s^2 \lambda^2}{\pi^3 d}\sum_{n=1}^{\infty}\sin^2\left(\frac{\pi n W}{\lambda}\right)\frac{1-\exp(-2\pi n d/\lambda)}{n^3} \tag{B31}$$

which is consistent with the result derived by Kooy and Enz [3] for $\mu = 1$ considering that $\frac{2W}{\lambda} - 1 = \langle M_z\rangle/M_s$ is the average relative out-of-plane magnetization and that the volume density of the energy is $E_{d,s}/V = 2\sigma_{d,s}/\lambda$. As noted by Johansen *et al.* [6], the sum can be written in terms of polylog functions:

$$\begin{aligned}4\sum_{n=1}^{\infty}\sin^2\left(\frac{\pi n W}{\lambda}\right)\frac{1-\exp(-2\pi n d/\lambda)}{n^3} &= -2\,\mathrm{Li}_3\left(e^{-\frac{2d\pi}{\lambda}}\right) + \mathrm{Li}_3\left(e^{\frac{2i\pi W}{\lambda}-\frac{2d\pi}{\lambda}}\right)\\ &\quad + \mathrm{Li}_3\left(e^{-\frac{2\pi d}{\lambda}-\frac{2i\pi W}{\lambda}}\right) - \mathrm{Li}_3\left(e^{\frac{2i\pi W}{\lambda}}\right) - \mathrm{Li}_3\left(e^{-\frac{2i\pi W}{\lambda}}\right) + 2\zeta(3).\end{aligned} \tag{B32}$$

A finite domain wall width Δ can be included in the model in exact analogy to the single stripe domain case by multiplication by $2\pi\,\hat{f}_1^{\,2}(k)$ in Fourier space. The convolution theorem holds also for discrete Fourier series. Hence, we obtain

$$\sigma_{d,s}^{N_{dw}=\infty,N_l=1} = \frac{\lambda}{4}\mu_0 M_s^2\left(\frac{2W}{\lambda} - 1\right)^2 + \frac{\pi\mu_0 M_s^2\Delta^2}{d}\sum_{n=1}^{\infty}\frac{\sin^2\left(\frac{\pi n W}{\lambda}\right)}{\sinh^2\left(\frac{\pi^2 n\Delta}{\lambda}\right)}\frac{1-\exp(-2\pi n d/\lambda)}{n}. \tag{B33}$$

3. Extension to multilayers

Consider a multilayer film with a multidomain stripe state containing walls of finite size. To find its surface stray field energy, we can use exactly the same approach as for the single layer film (B33). Multiplication of the explicit multilayer energy of a binary pattern given by Suna [13] and Draaisma [14] by a factor of $2\pi\,\hat{f}_1^{\,2}(k)$ in Fourier space results in

$$\begin{aligned}\sigma_{d,s}^{N_{dw}=\infty,N_l=\mathcal{N}} &= \frac{\lambda}{4}\mu_0 M_s^2\left(\frac{2W}{\lambda} - 1\right)^2\frac{\mathcal{T}}{\mathcal{P}} + \frac{\pi\mu_0 M_s^2\Delta^2}{\mathcal{P}}\sum_{n=1}^{\infty}\frac{\sin^2(\frac{\pi n W}{\lambda})}{n\sinh^2\left(\frac{\pi^2 n\Delta}{\lambda}\right)}\\ &\quad\times\left\{\frac{2\sinh\left(\frac{\pi n\mathcal{T}}{\lambda}\right)\sinh\left(\frac{\pi n(\mathcal{P}-\mathcal{T})}{\lambda}\right)}{\sinh\left(\frac{\pi n\mathcal{P}}{\lambda}\right)} + \frac{\sinh^2\left(\frac{\pi n\mathcal{T}}{\lambda}\right)}{\mathcal{N}\sinh^2\left(\frac{\pi n\mathcal{P}}{\lambda}\right)}\left[1-\exp\left(-\frac{2\pi\mathcal{P}\mathcal{N}n}{\lambda}\right)\right]\right\}.\end{aligned} \tag{B34}$$

The resulting expression for $\sigma_{d,s}^{\infty,\mathcal{N}}$ can be simplified under the condition $\lambda \gg \pi\mathcal{P}$, which is most often the case. By expanding the terms inside of the curly brackets of Eq. (B34) in Maclaurin series up to the first order in $\pi n\mathcal{T}/\lambda$ and $\pi n\mathcal{P}/\lambda$, we obtain

$$\begin{aligned}\sigma_{d,s}^{\infty,\mathcal{N}}\big|_{\lambda\gg\pi\mathcal{P}} &= \frac{\lambda}{4}\mu_0 M_s^2\left(1-\frac{2W}{\lambda}\right)^2\frac{\mathcal{T}}{\mathcal{P}} + \left[\frac{\pi\mu_0(M_s\mathcal{T}/\mathcal{P})^2\Delta^2}{(\mathcal{P}\mathcal{N})}\sum_{n=1}^{\infty}\frac{\sin^2\left(\frac{\pi n W}{\lambda}\right)}{\sinh^2\left(\frac{\pi^2 n\Delta}{\lambda}\right)}\frac{1-\exp(-2\pi n\mathcal{P}\mathcal{N}/\lambda)}{n}\right]\\ &\quad + \frac{2\pi^2\mu_0 M_s^2\Delta^2}{\lambda}\left[\frac{\mathcal{T}}{\mathcal{P}} - \left(\frac{\mathcal{T}}{\mathcal{P}}\right)^2\right]\sum_{n=1}^{\infty}\frac{\sin^2\left(\frac{\pi n W}{\lambda}\right)}{\sinh^2\left(\frac{\pi^2 n\Delta}{\lambda}\right)}.\end{aligned} \tag{B35}$$

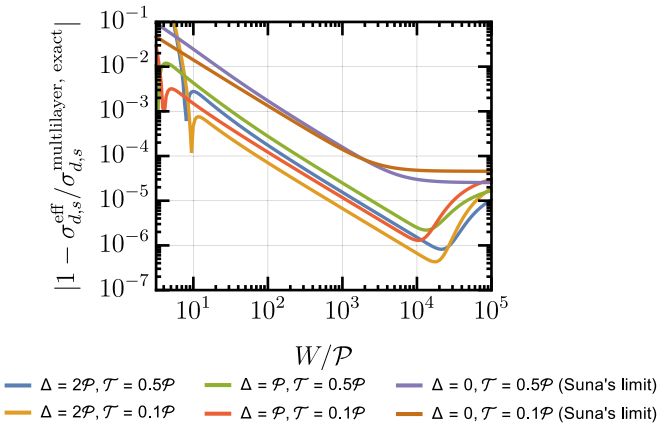

FIG. 11. The error of the effective medium model for the surface stray field energy of a demagnetized multilayer film with a multilayer period of $\mathcal{P} = 5$ nm and $\mathcal{N} = 10$ multilayer repetitions.

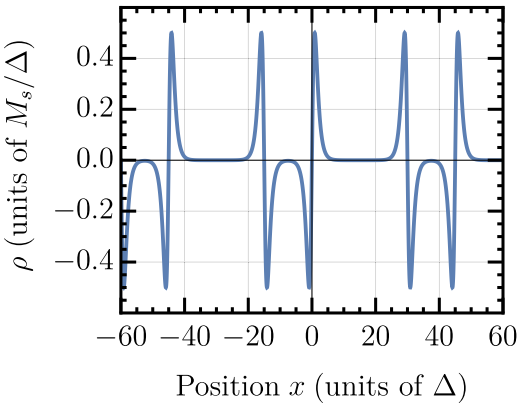

FIG. 12. Distribution of volume charges in single layer films with multidomain stripe state (with domain periodicity $\lambda = 45\Delta$ and minority domain size of $W = 15\Delta$) possessing Néel domain walls of fixed chirality.

Consider the function

$$F\left(\frac{\Delta}{\lambda},\frac{W}{\lambda}\right) = 8\pi^2\frac{\Delta^2}{\lambda^2}\sum_{n=1}^{\infty}\frac{\sin^2\left(\frac{\pi n W}{\lambda}\right)}{\sinh^2\left(\frac{\pi^2 n\Delta}{\lambda}\right)}. \tag{B36}$$

By performing the asymptotic analysis of F in the vicinity of $\Delta/\lambda = 0$, we obtain the following strict asymptotic relation: (See Fig. 10 for the error of such an approximation)

$$F \sim F_{\text{approx}} = \left(1-\frac{4\Delta}{\lambda}\right) - \left(1-\frac{2W}{\lambda}\right)^2 \quad \text{at } \Delta/\lambda \to 0. \tag{B37}$$

Here, the second and all the higher-order terms converge to zero as $\Delta/\lambda \to 0$.[6] Therefore, the surface stray field energy of a multilayer film finally becomes

$$\sigma^{\infty,\mathcal{N}}_{d,s}\big|_{\lambda\gg\pi\mathcal{P}} = \frac{\lambda}{4}\mu_0 M_s^2\left(1-\frac{2W}{\lambda}\right)^2\left(\frac{\mathcal{T}}{\mathcal{P}}\right)^2 + \left[\frac{\pi\mu_0(M_s\mathcal{T}/\mathcal{P})^2\Delta^2}{(\mathcal{P}\mathcal{N})}\sum_{n=1}^{\infty}\frac{\sin^2\left(\frac{\pi n W}{\lambda}\right)}{\sinh^2\left(\frac{\pi^2 n\Delta}{\lambda}\right)}\frac{1-\exp(-2\pi n\mathcal{P}\mathcal{N}/\lambda)}{n}\right]$$
$$+\frac{\mu_0 M_s^2 W}{2}\left(1-\frac{4\Delta}{W}\right)\left[\frac{\mathcal{T}}{\mathcal{P}}-\left(\frac{\mathcal{T}}{\mathcal{P}}\right)^2\right]. \tag{B38}$$

The error of the effective model of the demagnetized state is plotted on Fig. 11. As we can see, this model works very well even for intermediate and small domains as long as $W \gtrsim 10\mathcal{P}$.

APPENDIX C: VOLUME STRAY FIELD ENERGY CALCULATIONS

1. Stripe array and isolated wall states in single layer films

Consider a magnetized single layer film, in which $2\mathcal{M}-1$ domain walls of fixed chirality with transient wall angle ψ separate stripe domains of periodicity λ and width W of one of the domains. The calculation of the volume stray field energy of this state is accomplished by calculating the integral

$$\sigma_{d,v} = \frac{\mu_0}{8\pi L d(2\mathcal{M}-1)}\iint d^3\mathbf{r}\,d^3\mathbf{r}'\rho(\mathbf{r})\frac{1}{|\mathbf{r}-\mathbf{r}'|}\rho(\mathbf{r}') \tag{C1}$$

with the following volume charge distribution: (see Fig. 12)

$$\rho(\mathbf{r}) = \sum_{j=-\mathcal{M}+1}^{\mathcal{M}-1}[\rho_1(x-j\lambda,y,z)-\rho_1(x-j\lambda+W,y,z)], \tag{C2}$$

$$\rho_1(\mathbf{r}) = \rho_1(x)\theta(L/2-|y-L/2|)\theta(d/2-|z-d/2|), \tag{C3}$$

$$\rho_1(x) = -\nabla\cdot\mathbf{M} = \frac{M_s}{\Delta}\sin(\psi)\frac{\tanh(x/\Delta)}{\cosh(x/\Delta)}, \tag{C4}$$

where $\theta(x)$ is the Heaviside function, L is the width in the y direction, d is the film thickness, and Δ is the domain wall width.

By following the approach of Büttner *et al.* [17], we find in the limit $L \to \infty$ (compare with Eq. (24)

[6]The approximation (B37) is particularly accurate for the relevant case $W > 8\Delta$ as discussed in the main paper (see Fig. 11).

from [17])

$$\sigma_{d,v}^{1,1} = \frac{\mu_0}{8\pi d(2\mathcal{M}-1)} \sum_{m=-2\mathcal{M}+2}^{2\mathcal{M}-2} (2\mathcal{M}-1-|m|) \times \int_0^d dz \int_0^d dz' \int_{-\infty}^{+\infty} dx\, dx' \rho_1(x)\rho_1(x') \times [h_1(x-x'+m\lambda, z-z') - h_1(x-x'+m\lambda-W, z-z')], \tag{C5}$$

where

$$h_1(x,z) = \lim_{L\to\infty} \frac{1}{L} \int_0^L dy \int_0^L dy' \frac{1}{\sqrt{(y-y')^2+x^2+z^2}} = -\ln(x^2+z^2). \tag{C6}$$

To facilitate the calculations, we can use the following property of convolution:

$$\iint dx\, dx' f(x)g(x')h(x-x'+c) = \sqrt{2\pi} \int dk\, \hat{g}(k)\hat{h}(k)[\hat{f}(k)]^* e^{-ikc}, \tag{C7}$$

which can be derived by following the logic from [17]. Introducing

$$\zeta(x) = \frac{1}{\Delta} \frac{\tanh(x/\Delta)}{\cosh(x/\Delta)}, \tag{C8}$$

we have the following result for $2\mathcal{M}-1$ domain walls (compare with Eq. (29) from [17]):

$$\sigma_{d,v}^{N_{dw}=2\mathcal{M}-1, N_l=1} = \frac{\mu_0 M_s^2 \sqrt{2\pi} \sin^2(\psi)}{8\pi(2\mathcal{M}-1)d} \sum_{m=-2\mathcal{M}+2}^{2\mathcal{M}-2} (2\mathcal{M}-1-|m|) \tag{C9}$$

$$\iint_0^d dz\, dz' \int_{-\infty}^{+\infty} dk |\hat{\zeta}(k)|^2 \hat{h}(k, z-z') e^{-ik\lambda m}(1-e^{ikW}) = \frac{\mu_0 M_s^2 \Delta \sin^2(\psi)}{4t/2\pi} \sum_{m=-2\mathcal{M}+2}^{2\mathcal{M}-2} \left\{ \frac{2\mathcal{M}-1-|m|}{2\mathcal{M}-1} \times \int_0^{+\infty} dq \frac{e^{-qt/2\pi} + qt/2\pi - 1}{q\cosh^2(q/4)} \times \left[\cos\left(\frac{q\lambda m}{2\pi\Delta}\right) - \cos\left(\frac{q(\lambda m - W)}{2\pi\Delta}\right) \right] \right\}, \tag{C10}$$

where we introduced $q = 2\pi k\Delta$ and a reduced thickness $t = d/\Delta$. To simplify the expression (C10) we can swap the integral and sum symbols. By recognizing that the following sum can be expressed analytically as

$$\sum_{m=-2\mathcal{M}+2}^{2\mathcal{M}-2} (2\mathcal{M}-1-|m|)\{\cos(k\lambda m) - \cos[k(\lambda m - W)]\} = 2\sin^2\left(\frac{k\lambda}{2}(2\mathcal{M}-1)\right) \csc^2\left(\frac{k\lambda}{2}\right) \sin^2\left(\frac{kW}{2}\right), \tag{C11}$$

we can express the volume stray field energy of the multidomain state with $2\mathcal{M}-1$ domain walls as follows:

$$\sigma_{d,v}^{2\mathcal{M}-1,1} = \frac{\mu_0 M_s^2 \Delta \sin^2(\psi)}{4t/2\pi} \int_0^{+\infty} dq \times \frac{2\left(e^{-\frac{qt}{2\pi}} + \frac{qt}{2\pi} - 1\right) \sin^2\left(\frac{qW}{4\pi\Delta}\right) \sin^2\left(\frac{q\lambda}{4\pi\Delta}(2\mathcal{M}-1)\right)}{q\cosh^2(q/4)(2\mathcal{M}-1)\sin^2\left(\frac{q\lambda}{4\pi\Delta}\right)}. \tag{C12}$$

In the limit of a regular stripe domain array $2\mathcal{M}-1 \to \infty$,

$$\sigma_{d,v}^{\infty,1} = \lim_{\mathcal{M}\to\infty} \sigma_{d,v}^{2\mathcal{M}-1,1} = \frac{\mu_0 M_s^2 \Delta \sin^2(\psi)}{2t/2\pi} \lim_{\mathcal{M}\to\infty} \int_0^{+\infty} dq \left\{ \frac{e^{-\frac{qt}{2\pi}} + \frac{qt}{2\pi} - 1}{q\cosh^2(q/4)} \times \frac{\sin^2\left(\frac{qW}{4\pi\Delta}\right) \sin^2\left(\frac{q\lambda}{4\pi\Delta}(2\mathcal{M}-1)\right)}{(2\mathcal{M}-1)\sin^2\left(\frac{q\lambda}{4\pi\Delta}\right)} \right\}. \tag{C13}$$

Swapping the limit and integral symbols should be carefully performed, as the function under the integral lacks the property of uniform convergence, which would erroneously lead to the conclusion that $\sigma_{d,v}^{\infty,1} = 0$. Instead, we substitute the function under the integral with the Dirac comb function

$$\lim_{\mathcal{M}\to\infty} \frac{\sin^2\left(\frac{q\lambda}{4\pi\Delta}(2\mathcal{M}-1)\right)}{(2\mathcal{M}-1)\sin^2\left(\frac{q\lambda}{4\pi\Delta}\right)} = \frac{4\pi^2\Delta}{\lambda} \sum_{n=0}^{\infty} \delta\left(q - \frac{4\pi^2\Delta}{\lambda}n\right). \tag{C14}$$

The equivalence of both functions in the limit $\mathcal{M}\to\infty$ is proved in Appendix E. Thus, we have

$$\sigma_{d,v}^{\infty,1} = \frac{\mu_0 M_s^2 \Delta \sin^2(\psi)}{2t/2\pi} \frac{4\pi^2\Delta}{\lambda} \sum_{n=0}^{\infty} \int_0^{+\infty} dq \times \sin^2\left(\frac{qW}{4\pi\Delta}\right) \frac{e^{-\frac{qt}{2\pi}} + \frac{qt}{2\pi} - 1}{q\cosh^2(q/4)} \delta\left(q - \frac{4\pi^2\Delta}{\lambda}n\right). \tag{C15}$$

By using the property of the delta function $\int \delta(x-x_0)f(x)dx = f(x_0)$, we finally obtain

$$\sigma_{d,v}^{\infty,1} = \frac{\pi\mu_0 M_s^2 \Delta^2 \sin^2(\psi)}{d} \times \sum_{n=1}^{\infty} \frac{\sin^2\left(\frac{\pi n W}{\lambda}\right)}{\cosh^2\left(\frac{\pi^2 n\Delta}{\lambda}\right)} \frac{\exp\left(-\frac{2\pi nd}{\lambda}\right) + \frac{2\pi nd}{\lambda} - 1}{n}. \tag{C16}$$

As a side note, the derived expression for the volume stray field energy of the multidomain state intrinsically contains both the self-interaction contribution $\sigma_{d,v}^{1,1}$ as well as the interaction term $\Delta\sigma_{d,v}^{\infty,1} = \sigma_{d,v}^{\infty,1} - \sigma_{d,v}^{1,1}$, responsible for the interaction between different domain walls. The self-interaction term $\sigma_{d,v}^{1,1}$ can be found by plugging $\mathcal{M}=1$ into Eq. (C10) and looks as follows [17]:

$$\sigma_{d,v}^{1,1} = \frac{\pi\mu_0 M_s^2 \Delta^2 \sin^2(\psi)}{2d} G\left(\frac{d}{2\pi\Delta}\right). \tag{C17}$$

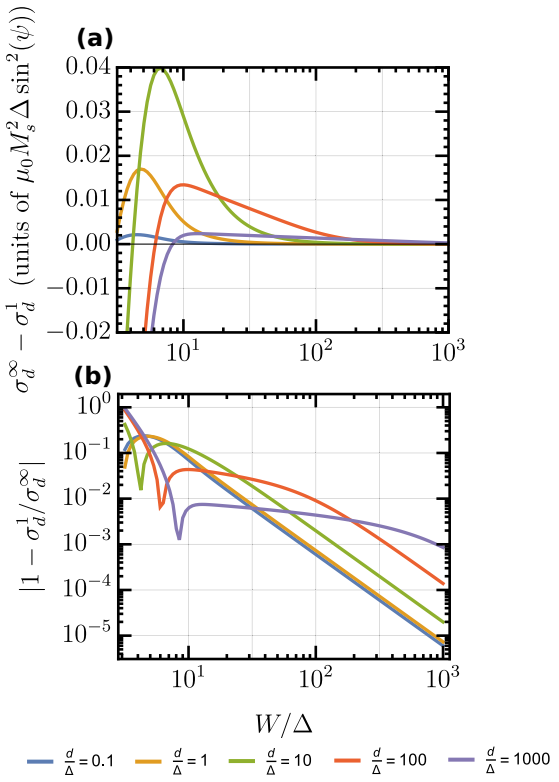

FIG. 13. The interaction term $\Delta\sigma_{d,v}^{\infty,1} = \sigma_{d,v}^{\infty,1} - \sigma_{d,v}^{1,1}$ for the single layer film with a demagnetized state $W_{\min} = W_{\mathrm{maj}} = \lambda/2$, which characterizes the difference between the volume stray field energy of the multidomain state with finite walls and the energy of the isolated Néel wall state. (a) The absolute magnitude and (b) the relative value. The tipping point in (b) corresponds to the change from a repelling behavior of domain walls (at large and intermediate domain width) to an attractive behavior (at small domain width).

The interaction term $\Delta\sigma_{d,v}^{\infty,1}$ results in a positive value for large domains, and in negative values for very small domains. The latter is caused by the overlapping tails from the neighboring domain walls, which creates finite volume charges of the opposite signs inside of the neighboring domains. The interaction term is negligible when $W \gg 2\pi\Delta$, so a fair approximation for $\sigma_{d,v}^{\infty,1}$ would be a single self-interaction term $\sigma_{d,v}^{1,1}$ from Eq. (C17). However, the same treatment for domains of intermediate and small size (when $W < 50\Delta$) would result in significant energy underestimations, so the explicit Eq. (C16) must be used there (see Fig. 13).

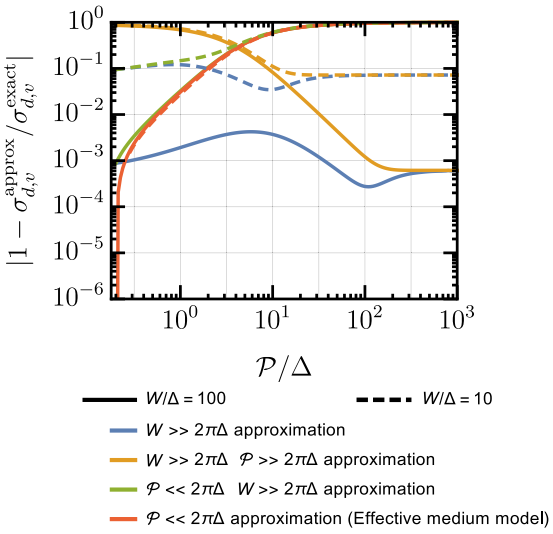

FIG. 14. The error of various approximations to the exact multilayer multidomain volume stray field energy as a function of multilayer period $\mathcal{P}$ and domain width W for a system with single magnetic layer thickness $\mathcal{T} = 0.2\Delta$ and $\mathcal{N} = 10$ multilayer repetitions.

2. Extension to multilayers

The multilayer volume stray field energy for an isolated domain wall $\sigma_{d,v}^{1,\mathcal{N}}$ has already been calculated in Ref. [17]:

$$\sigma_{d,v}^{N_{dw}=1,N_l=\mathcal{N}} = \frac{\mu_0 M_s^2 \Delta \sin^2(\psi)}{8p/2\pi} \sum_{i=-\mathcal{N}+1}^{\mathcal{N}-1} \frac{\mathcal{N}-|i|}{\mathcal{N}} \times \left[G\left(\left|\frac{ip+t}{2\pi}\right|\right) + G\left(\left|\frac{ip-t}{2\pi}\right|\right) - 2G\left(\left|\frac{ip}{2\pi}\right|\right)\right], \tag{C18}$$

where $t = \mathcal{T}/\Delta$ is the reduced single magnetic layer thickness, $p = \mathcal{P}/\Delta$ is the reduced multilayer periodicity. Incorporating the results of the previous subsection, we can modify Eq. (C18) to characterize a magnetized multidomain state with $\mathcal{N}$ layer repeats and $2\mathcal{M}-1$ domain walls:

$$\sigma_{d,v}^{2\mathcal{M}-1,\mathcal{N}} = \frac{\mu_0 M_s^2 \Delta \sin^2(\psi)}{8p/2\pi} \sum_{i=-\mathcal{N}+1}^{\mathcal{N}-1} \frac{\mathcal{N}-|i|}{\mathcal{N}} \sum_{m=-2\mathcal{M}+2}^{2\mathcal{M}-2} \frac{2\mathcal{M}-1-|m|}{2\mathcal{M}-1} \left[\tilde{G}\left(\left|\frac{ip+t}{2\pi}\right|, \frac{ml}{2\pi}, \frac{w}{2\pi}\right) + \tilde{G}\left(\left|\frac{ip-t}{2\pi}\right|, \frac{ml}{2\pi}, \frac{w}{2\pi}\right) - 2\tilde{G}\left(\left|\frac{ip}{2\pi}\right|, \frac{ml}{2\pi}, \frac{w}{2\pi}\right)\right], \tag{C19}$$

$$\tilde{G}(\alpha,\beta,\gamma) = \int_0^{+\infty} dq \frac{e^{-q\alpha} + q\alpha - 1}{q\cosh^2(q/4)} \{\cos(\beta q) - \cos[(\beta-\gamma)q]\}, \tag{C20}$$

where $l = \lambda/\Delta$ is the reduced domain periodicity, $w = W/\Delta$ is the reduced domain size. The integral (C20) has an analytical solution, though a lengthy one. However, we can instead incorporate the derived solution (C16) for single layer films with an

infinite number of domain walls into Eq. (C19) and thus eliminate the sum over m:

$$\sigma_{d,v}^{\infty,\mathcal{N}} = \frac{\pi\mu_0 M_s^2\Delta^2\sin^2(\psi)}{2\mathcal{P}}\sum_{i=-\mathcal{N}+1}^{\mathcal{N}-1}\frac{\mathcal{N}-|i|}{\mathcal{N}}\sum_{n=1}^{\infty}\frac{\sin^2\left(\frac{\pi nW}{\lambda}\right)}{n\cosh^2(\frac{\pi^2 n\Delta}{\lambda})}$$
$$\times\left[e^{-\frac{2\pi n|i\mathcal{P}+\mathcal{T}|}{\lambda}}+e^{-\frac{2\pi n|i\mathcal{P}-\mathcal{T}|}{\lambda}}-2e^{-\frac{2\pi n|i\mathcal{P}|}{\lambda}}+\frac{2\pi n|i\mathcal{P}+\mathcal{T}|}{\lambda}+\frac{2\pi n|i\mathcal{P}-\mathcal{T}|}{\lambda}-2\frac{2\pi n|i\mathcal{P}|}{\lambda}\right]. \tag{C21}$$

After using the symmetry $i\to -i$ to remove the modulus symbol and swapping the sums in Eq. (C21) we obtain

$$\sigma_{d,v}^{\infty,\mathcal{N}} = \frac{\pi\mu_0 M_s^2\Delta^2\ \sin^2(\psi)}{2\mathcal{P}\mathcal{N}}\sum_{n=1}^{\infty}\frac{\sin^2\left(\frac{\pi nW}{\lambda}\right)}{n\cosh^2\left(\frac{\pi^2 n\Delta}{\lambda}\right)}\left\{2\mathcal{N}\left(e^{-\frac{2\pi n\mathcal{T}}{\lambda}}+\frac{2\pi n\mathcal{T}}{\lambda}-1\right)\right.$$
$$\left.+\ 2\sum_{i=1}^{\mathcal{N}-1}(\mathcal{N}-i)\left[e^{-\frac{2\pi n(i\mathcal{P}+\mathcal{T})}{\lambda}}+e^{-\frac{2\pi n(i\mathcal{P}-\mathcal{T})}{\lambda}}-2e^{-\frac{2\pi ni\mathcal{P}}{\lambda}}\right]\right\}. \tag{C22}$$

Finally, using the property of sums

$$\sum_{i=1}^{\mathcal{N}-1}(\mathcal{N}-i)e^{-i\beta} = \frac{e^{-\beta\mathcal{N}}[e^{\beta}+e^{\beta(\mathcal{N}+1)}(\mathcal{N}-1)-\mathcal{N}e^{\beta\mathcal{N}}]}{(e^{\beta}-1)^2}, \tag{C23}$$

we can simplify the expression even further with the following final result:

$$\sigma_{d,v}^{\infty,\mathcal{N}} = \frac{\pi\mu_0 M_s^2\Delta^2\ \sin^2(\psi)}{\mathcal{N}\mathcal{P}}\sum_{n=1}^{\infty}\frac{\sin^2\left(\frac{\pi nW}{\lambda}\right)}{n\cosh^2\left(\frac{\pi^2 n\Delta}{\lambda}\right)}\left\{\mathcal{N}\left(e^{-\frac{2\pi n\mathcal{T}}{\lambda}}+\frac{2\pi n\mathcal{T}}{\lambda}-1\right)\right.$$
$$\left.+\ \frac{e^{-\frac{2\pi n(\mathcal{P}\mathcal{N}+\mathcal{T})}{\lambda}}\left(e^{\frac{2\pi n\mathcal{T}}{\lambda}}-1\right)^2}{\left(e^{\frac{2\pi n\mathcal{P}}{\lambda}}-1\right)^2}\left(e^{\frac{2\pi n\mathcal{P}}{\lambda}}+e^{\frac{2\pi n\mathcal{P}(\mathcal{N}+1)}{\lambda}}(\mathcal{N}-1)-\mathcal{N}e^{\frac{2\pi n\mathcal{N}\mathcal{P}}{\lambda}}\right)\right\}. \tag{C24}$$

The expression (C24) is the exact volume stray field energy of multilayers with a magnetized multidomain state and finite transient walls with a fixed angle ψ. However, it can be simplified in many experimentally relevant cases as follows:

$$\sigma_{d,v}^{\infty,\mathcal{N}} = \begin{cases}\sigma_{d,v}^{1,\mathcal{N}}, & \text{if } \lambda\gg\Delta\\ \sigma_{d,v}^{1,1}, & \text{if } \lambda,\mathcal{P}/2\pi\gg\Delta\\ \left(\frac{\mathcal{T}}{\mathcal{P}}\right)^2\sigma_{d,v}^{1,1}(d=\mathcal{N}\mathcal{P}), & \text{if } \mathcal{P}\ll 2\pi\Delta\ll 2\pi\lambda\\ \left(\frac{\mathcal{T}}{\mathcal{P}}\right)^2\sigma_{d,v}^{\infty,1}(d=\mathcal{N}\mathcal{P}), & \text{if } \mathcal{P}\ll 2\pi\Delta,\lambda/2\pi\end{cases} \tag{C25}$$

where $\sigma_{d,v}^{1,\mathcal{N}}$ is the energy of the isolated wall in a multilayer structure (C18). The last two cases represent an effective medium approach, in which the saturation magnetization scales with scaling factor $\mathcal{T}/\mathcal{P}$. Very often real multilayer structures operate in this regime. All the mentioned cases are depicted in Fig. 14.

Let us prove the effective medium treatment for volume charge interactions. Assuming $\mathcal{P}\ll\frac{\lambda}{2\pi}$ and, hence, $\mathcal{T}\ll\frac{\lambda}{2\pi}$, we can expand the expression in curly brackets of Eq. (C24) in Maclaurin series around $2\pi n\mathcal{T}/\lambda=0$ and $2\pi n\mathcal{P}/\lambda=0$. The expansion results in

$$\sigma_{d,v}^{N_{dw}=\infty,N_l=\mathcal{N}} \to \frac{\pi\mu_0 M_s^2\Delta^2\ \sin^2(\psi)}{\mathcal{N}\mathcal{P}}\sum_{n=1}^{\infty}\frac{\sin^2\left(\frac{\pi nW}{\lambda}\right)}{n\cosh^2\left(\frac{\pi^2 n\Delta}{\lambda}\right)}\frac{\mathcal{T}^2}{\mathcal{P}^2}\left[\frac{1}{2}\left(\frac{2\pi n\mathcal{P}}{\lambda}\right)^2-\frac{1}{6}\left(\frac{2\pi n\mathcal{P}}{\lambda}\right)^3+\frac{1}{24}\left(\frac{2\pi n\mathcal{P}}{\lambda}\right)^4\right.$$
$$\left.-\frac{1}{120}\left(\frac{2\pi n\mathcal{P}}{\lambda}\right)^5+\ldots\right]+\frac{\mathcal{T}^2}{\mathcal{P}^2}\left[\frac{4}{3}\frac{\pi^3\mathcal{P}^3 n}{\lambda^3}+\mathcal{O}\left(\frac{\mathcal{P}^4 n^2}{\lambda^4}\right)\right]. \tag{C26}$$

Recognizing that the expression inside the first brackets represents the expansion of an exponent around zero without its first two terms, we can reduce the expression to a single layer-like form[7]

$$\sigma_{d,v}^{\infty,\mathcal{N}} \to \frac{\pi\mu_0 M_s^2\Delta^2\ \sin^2(\psi)}{\mathcal{N}\mathcal{P}}\left(\frac{\mathcal{T}}{\mathcal{P}}\right)^2\sum_{n=1}^{\infty}\left\{\frac{\sin^2\left(\frac{\pi nW}{\lambda}\right)}{\cosh^2\left(\frac{\pi^2 n\Delta}{\lambda}\right)}\frac{e^{-\frac{2\pi n\mathcal{P}\mathcal{N}}{\lambda}}+\frac{2\pi n\mathcal{P}\mathcal{N}}{\lambda}-1}{n}+\mathcal{O}\left(\frac{\mathcal{P}^3 n}{\lambda^3}\right)\right\}. \tag{C27}$$

[7]For large n, the denominator in the sum increases $\sim\exp(\alpha n)$, which makes the sum converge quickly.

APPENDIX D: DISCRETE FOURIER SPACE IDENTITIES

Let $g(x)$ be a real-valued function with a discrete representation in Fourier space:

$$g(x) = \sum_k \hat{g}_k e^{ikx} = \sum_k \hat{g}_k^* e^{-ikx} \tag{D1}$$

with $\hat{g}_k$ being the Fourier coefficients of g. Now, assume we wish to calculate the following integral:

$$I = \iint dx\, dx' g(x) g(x') h(x - x') \tag{D2}$$

with some function h. We can write the integral as

$$I = \iint dx\, dx' \sum_k \hat{g}_k \hat{g}_k^* e^{ik(x-x')} h(x - x') \tag{D3}$$

$$= \sum_k |\hat{g}_k|^2 \iint dx\, dx' e^{ik(x-x')} h(x - x') \tag{D4}$$

$$= \sum_k |\hat{g}_k|^2 \iint dx\, dy\, e^{iky} h(y) \tag{D5}$$

$$= \sum_k |\hat{g}_k|^2 \int dx \sqrt{2\pi} \hat{h}(k) \tag{D6}$$

$$= \sqrt{2\pi} \sum_k |\hat{g}_k|^2 \hat{h}(k) \int dx \tag{D7}$$

$$= \sqrt{2\pi} N\lambda \sum_k |\hat{g}_k|^2 \hat{h}(k), \tag{D8}$$

where N is the number of periods in along the x dimension (which we will set to infinity at a later stage) and λ is the period length, so $N\lambda$ is the total length of the sample. Note that there are no restrictions on which values of k we are summing over. $\hat{h}$ is the regular, continuous Fourier transform of h, which is evaluated at the discrete values of k. For the particular case of $g(x) = 1$ and h as in Eq. (B9), we get $I = -2\pi d N\lambda$, which is consistent with the volume energy density $\frac{E}{V} = \frac{2\sigma}{N\lambda} = \frac{2\mu_0 M_s^2 I(g=1)}{8\pi d N\lambda} = \frac{1}{2}\mu_0 M_s^2$ of a homogeneously magnetized film.

APPENDIX E: DIRAC COMB

Consider a function $Z(q)$:

$$Z(q) = \lim_{\mathcal{N}\to\infty} \frac{1}{\mathcal{N}} \frac{\sin^2(qa\mathcal{N})}{\sin^2(qa)}, \tag{E1}$$

where $\mathcal{N} = 2\mathcal{M} - 1$ is an odd number. Such a function contains critical points at $q = \frac{\pi n}{a}$. Note that at the critical points the following holds true:

$$\lim_{q\to\frac{\pi n}{a}} \frac{1}{\mathcal{N}} \frac{\sin^2(qa\mathcal{N})}{\sin^2(qa)} = \mathcal{N}, \tag{E2}$$

where we have applied the L'Hospital's rule twice for Eq. (E2). Thus, evaluating $Z(q)$ we obtain the following:

$$Z(q) = \lim_{\mathcal{N}\to\infty} \frac{1}{\mathcal{N}} \frac{\sin^2(qa\mathcal{N})}{\sin^2(qa)} = \begin{cases} \infty, & \text{if } q = \frac{\pi n}{a} \\ 0, & q \in \left(\frac{\pi n}{a} - \epsilon, \frac{\pi n}{a} + \epsilon\right). \end{cases} \tag{E3}$$

Note that $Z(q)$ can also be integrated around critical points, resulting in

$$\int_{\frac{\pi n}{a}-\epsilon}^{\frac{\pi n}{a}+\epsilon} Z(q) dq = \frac{\pi}{a}. \tag{E4}$$

Therefore, a normalized function $Z(q)/\frac{\pi}{a}$, when evaluated around its critical points, repeats the properties of the delta function. Hence, $Z(q)$ in the entire range $q \in [0,\infty)$ can be expressed as the Dirac comb function:

$$Z(q) = \frac{\pi}{a} \sum_{n=0}^{\infty} \delta\left(q - \frac{\pi n}{a}\right). \tag{E5}$$

[1] C. Kittel, Phys. Rev. **70**, 965 (1946).
[2] J. A. Cape and G. W. Lehman, J. Appl. Phys. **42**, 5732 (1971).
[3] C. Kooy and U. Enz, Philips Res. Rep. **15**, 7 (1960).
[4] O. Hellwig, A. Berger, J. B. Kortright, and E. E. Fullerton, J. Magn. Magn. Mater. **319**, 13 (2007).
[5] V. Kamberský, P. De Haan, J. Šimšová, S. Porthun, R. Gemperle, and J. C. Lodder, J. Magn. Magn. Mater. **157-158**, 301 (1996).
[6] T. H. Johansen, A. V. Pan, and Y. M. Galperin, Phys. Rev. B **87**, 060402 (2013).
[7] C. Moreau-Luchaire, C. Moutafis, N. Reyren, J. Sampaio, C. A. F. Vaz, N. Van Horne, K. Bouzehouane, K. Garcia, C. Deranlot, P. Warnicke, P. Wohlhüter, J.-M. George, M. Weigand, J. Raabe, V. Cros, and A. Fert, Nat. Nanotechnol. **11**, 444 (2016).
[8] S. Woo, K. Litzius, B. Krüger, M.-Y. Im, L. Caretta, K. Richter, M. Mann, A. Krone, R. M. Reeve, M. Weigand, P. Agrawal, I. Lemesh, M.-A. Mawass, P. Fischer, M. Kläui, and G. S. D. Beach, Nat. Mater. **15**, 501 (2016).
[9] I. Dzyaloshinsky, J. Phys. Chem. Solids **4**, 241 (1958).
[10] T. Moriya, Phys. Rev. **120**, 91 (1960).
[11] A. Bogdanov and D. Yablonskii, Zh. Eksp. Teor. Fiz. **95**, 178 (1989).
[12] Z. Málek and V. Kamberský, Czech. J. Phys. **8**, 416 (1958).
[13] A. Suna, J. Appl. Phys. **59**, 313 (1986).
[14] H. J. G. Draaisma and W. J. M. De Jonge, J. Appl. Phys. **62**, 3318 (1987).
[15] G. P. Zhao, L. Chen, and J. Wang, J. Appl. Phys. **105**, 061601 (2009).
[16] F. Virot, L. Favre, R. Hayn, and M. D. Kuz'min, J. Phys. D: Appl. Phys. **45**, 405003 (2012).
[17] F. Büttner, B. Krüger, S. Eisebitt, and M. Kläui, Phys. Rev. B **92**, 054408 (2015).
[18] R. Skomski, H.-P. Oepen, and J. Kirschner, Phys. Rev. B **58**, 3223 (1998).
[19] A. Thiaville, J. M. García, and J. Miltat, J. Magn. Magn. Mater. **242-245**, 1061 (2002).
[20] M. T. Johnson, P. J. H. Bloemen, F. J. a. D. Broeder, and J. J. D. Vries, Rep. Prog. Phys. **59**, 1409 (1996).
[21] A. Bogdanov and A. Hubert, J. Magn. Magn. Mater. **138**, 255 (1994).

[22] A. Vansteenkiste, J. Leliaert, M. Dvornik, M. Helsen, F. Garcia-Sanchez, and B. Van Waeyenberge, AIP Adv. **4**, 107133 (2014).
[23] S. Rohart and A. Thiaville, Phys. Rev. B **88**, 184422 (2013).
[24] O. Hellwig, G. P. Denbeaux, J. B. Kortright, and E. E. Fullerton, Phys. B (Amsterdam) **336**, 136 (2003).
[25] J. Miguel, J. F. Peters, O. M. Toulemonde, S. S. Dhesi, N. B. Brookes, and J. B. Goedkoop, Phys. Rev. B **74**, 094437 (2006).
[26] H. B. Braun, Phys. Rev. B **50**, 16485 (1994).